

# Correlations of Electronic and Chemical State on $\text{La}_{0.7}\text{Sr}_{0.3}\text{MnO}_3$ Dense Thin-Film Cathode Surfaces

K. Katsiev<sup>1</sup>, B. Yildiz<sup>1</sup>, B. Kavaipatti<sup>2</sup>, and P. Salvador<sup>2</sup>

<sup>1</sup>Department of Nuclear Science and Engineering, Massachusetts Institute of Technology, Cambridge, MA 02139, USA.

<sup>2</sup>Department of Materials Science and Engineering, Carnegie Mellon University, Pittsburgh, PA 15213, USA.

We report on the surface topography, electron tunneling and chemical characteristics of 10nm- and 50nm-thick  $\text{La}_{0.7}\text{Sr}_{0.3}\text{MnO}_3$  (LSM) thin-films at temperatures up to 580°C in  $10^{-3}$  mbar oxygen pressure, using *in situ* scanning tunneling microscopy and spectroscopy (STM/STS). Coarsening of the grains was found on the 10nm-thick LSM film. High resolution mapping of the tunneling spectra onto the surface topography showed a higher electron exchange rate at select grain boundaries compared to grain surfaces. A threshold-like drop in the tunneling current was observed at positive bias in STS, and is suggested as a unique indicator to the activation polarization in cation-oxygen bonding on LSM. Sr-enrichment and Mn-depletion were found on the surface at high temperature using Auger electron spectroscopy, accompanied by a reduction in tunneling conductance in STS. This suggests that the Mn-terminated surfaces are more active for electron exchange in oxygen reduction compared to the (La,Sr)-terminated surfaces on LSM.

## Introduction

Perovskite type mixed ionic-electronic conductor (MIEC) oxides are widely used as Solid Oxide Fuel Cell (SOFC) cathodes (1). It is well-known that their surface structure plays an important role in the electrocatalytic activity for oxygen reduction (OR) (2, 3). A particularly interesting material in this context is  $\text{La}_{0.7}\text{Sr}_{0.3}\text{MnO}_3$  (LSM) (4, 5) – an MIEC with poor ionic conductivity. Main obstacles to a widespread use of SOFCs thus far are materials degradation at the high operating temperatures or poor activity of the cathode if lowering of temperatures attempted. A major limitation of the cathode performance at lowered temperatures is the slow kinetics of the oxygen exchange on the perovskite oxide surfaces. The underlying OR mechanisms involving electronic and ionic charge transport on SOFC cathodes are not fully understood, and the impact of the different metal cations on the catalytic properties of the surface remains unclear. Thus, a fundamental understanding of the surface electronic and chemical state and its relation to the oxygen reduction at the atomistic level is essential for the development of cathodes with enhanced electrocatalytic activity.

In the present study, we investigated the surface topography, electron tunneling properties, and chemical characteristics on  $\text{La}_{0.7}\text{Sr}_{0.3}\text{MnO}_3$  (LSM) dense thin-film model cathodes. Two primary investigations reported here focused on: 1) the role of the structural inhomogeneities, such as grain boundaries or defect clusters, on the electronic properties of the surface, 2) the correlation between the surface chemical composition

and the surface electronic and ionic exchange characteristics of LSM. The findings of this investigation can help gain a more profound understanding of the oxygen reduction mechanism at the atomistic scale on the LSM cathodes.

### Experimental Approach

We deployed a new *in situ* approach combining surface sensitive probes of electronic structure and chemical state on the dense thin film cathodes – scanning tunneling microscopy and spectroscopy (STM/STS) and Auger Electron Spectroscopy (AES). Utilizing these surface sensitive probes, particularly the STM/STS, at high temperature and non-UHV conditions is unique, and makes it possible to relate the chemical and electronic state of the model cathode surfaces closely to the reacting environment of operational SOFC cathodes.

La<sub>0.7</sub>Sr<sub>0.3</sub>MnO<sub>3</sub> polycrystalline dense thin films with thicknesses of 10-100nm were grown on single crystal (111) Yttrium stabilized Zirconia YSZ by pulsed laser deposition (PLD) at 800°C in 50 mTorr of O<sub>2</sub>, and subsequently cooled to room temperature in 300 Torr O<sub>2</sub> (6). The results on the 10nm and 50nm-thick LSM films are reported here.

The *in situ* sample preparation, structural and compositional characterization is performed in the commercial UHV system (Omicron GmbH) consisting of a preparation and an analysis chamber with base pressure in the low 10<sup>-10</sup> mbar range. The preparation chamber is equipped with an ion-gun for sample cleaning, and a manipulator with a radiative heater. In addition, the chamber has one and four socket e-beam evaporators, and a residual gas analyzer. The analysis chamber is equipped with a variable-temperature AFM/STM (Omicron VT25 AFM design), retractable low-energy electron diffraction optics (LEED), electron gun and a cylindrical mirror energy analyzer (CMA) for Auger spectroscopy (AES). AES were acquired using normal incidence 4800eV electron beam.

The as-grown films were cleaned in ultrasonic bath with 99.99% purity ethyl alcohol, followed by Ar blow drying. In order to avoid altering the surface morphology and chemistry of samples from their as-grown state, e.g. by sputtering and annealing cycles, sample cleaning for the STM experiments was performed by heating the samples in oxygen for 30 min at 5x10<sup>-7</sup> mbar in the UHV chamber. This resulted in a significant reduction of the carbon deposits below the detection limit of AES energy analyzer.

During the cleaning of the samples in oxygen, the high-temperature STM/STS, and the AES experiments, the sample was radiatively heated by using Pyrolytic Boron Nitride (PBN) heater. 10<sup>-3</sup> mbar oxygen pressure localized in the vicinity of the sample's surface was created during the STM/STS measurements via direct oxygen dosing by a retractable dozer equipped with high precision leak valve.

Scanning tunneling microscopy at room temperature and high temperatures was performed in the constant-current mode using Pr/Ir tips, with the tunneling current, *I*, in 0.1-1nA range and sample at a bias voltage, *V*, in the range from -1V to 3V. A particular challenge in obtaining STM images at high temperatures was to determine the correct loop gain and Z-input gain for the piezo control, i.e. the signal amplification value of the

z-piezo of the STM. It has been crucial to set these parameters correctly in order to accommodate continuous changes in the tip-sample separation due to thermal expansion of the sample at elevated temperatures.

Scanning tunneling spectra were measured with the bias voltage from -3V to 3V in 20mV steps, with an acquisition time of 0.6 or 20ms per voltage step for the I-V and dI/dV data, respectively. To improve the quality of the STS data, which usually had dispersion in data points, all the I-V curves discussed here were averaged over the few tens of subsequent measurements.

## Results and Discussion

### Surface Topography at Ambient and Elevated Temperatures

The STM performed on the 10 and 50nm-thick LSM dense thin-films at room temperature (Fig. 1(a-d)) showed a textured surface structure. Two types of grains coexist without an apparent crystallographic orientation. First is the large flat island-type grains, with an average size of 100nm and 70nm on the 10nm- and 50nm-thick films, respectively, exhibiting clearly distinguishable step edges even at high-temperature imaging. Second type comprises the smaller grains, with an average size of 20nm and 35 nm. The overall peak-to-valley height difference is 4nm for the 10nm- and 6nm for the 50nm-thick films.

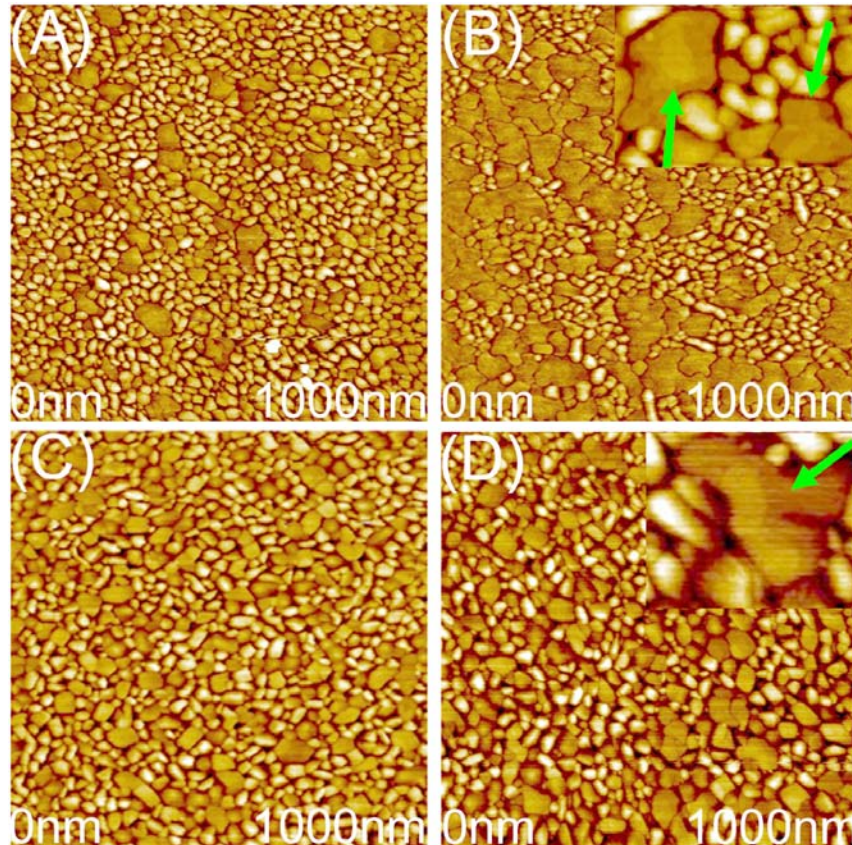


**Figure 1.**  $1 \times 1 \mu\text{m}^2$  topography of the (a,b) 10nm- and (c,d) 50nm-thick thin-film LSM surface, imaged with tunneling conditions of 2V and 1nA, at (a,c) room temperature, and (b,d) 580°C,  $P_{\text{O}_2}=10^{-3}$  mbar. The insets in (b,d),  $195 \times 130\text{nm}^2$  and  $164 \times 137\text{nm}^2$ , respectively, show the step-edge resolution (marked with arrows) on the island-type flat grains at high temperature.

Grain coarsening occurred on the 10nm-thick LSM film upon annealing at 580°C in oxygen pressure of  $10^{-3}$  mbar during STM/STS experiments lasting up to 24 hours. The coarsening resulted in the significantly increased fraction of the island-type grains (Fig. 1(b)). Contrary to this, the structure of the 50nm film did not evidently change via grain coarsening or surface roughening upon heating (Fig.1(d)).

### Surface Electronic Properties at Ambient and Elevated Temperatures

The optimized conditions allowing for high resolution imaging, down to step-edges as show in Fig. 1, at high temperature in non-UHV environment enabled the STS measurements to stably probe the electronic properties of the LSM surface. In the following sections, we report on the: 1) higher (compared to the grain surface) tunneling conductance at grain boundaries, 2) correlation of the surface composition and electron tunneling characteristics, 3) variations in the I/V behavior due to surface defects and the coexistence of different phases at the surface, and 4) threshold-like drop in the tunneling current at a positive bias as a manifestation of oxygen adsorption at the surface.

Correlation of Topography and Electronic Tunneling: The fine-resolution mapping of the tunneling current on the LSM surface obtained with STS at room temperature demonstrate a clear correlation between the surface topography (Fig.2 (A)) and the electron tunneling characteristics (Fig.2 (B)). The dark regions in Fig. 2(B) that are associated with the higher tunneling conductance mainly correspond to select grain boundaries in Fig.2 (A).

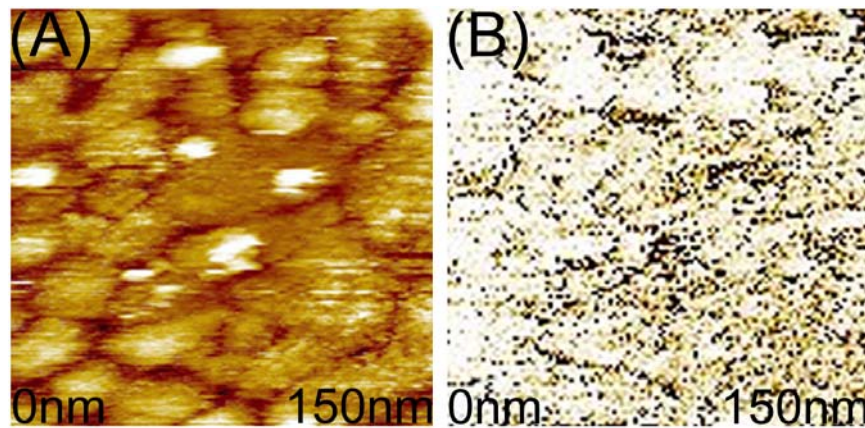


**Figure 2.** (A) Constant current STM image of 10nm LSM film surface (2V and 0.2nA) taken simultaneously with the tunneling spectroscopy map, and (B) the corresponding tunneling current map (on the same area in A) at -2.2V. Dark regions in (B), visible at some grain boundaries, represent higher tunneling current, and thus imply higher activity in electron exchange at select interfaces.

Considerably higher tunneling conductance at select grain boundaries compared to grain surfaces can be explained by the possible changes in the chemical composition due to segregation or structural distortions at the boundaries. Since the electronic conductance of the LSM is associated with the Mn cation reduction state (as discussed in the next section), the higher activity at the boundaries could result from the altered composition involving Mn enrichment. An increased diffusion constant and surface oxygen exchange rate was implied from the secondary ion mass spectroscopy (SIMS) results reported on the  $(La_{0.8}Sr_{0.2})(Mn_{1-y}Fe_y)O_{3\pm\delta}$  thin films and LSM powders (7, 8).

While SIMS is not a direct probe of the interfaces thus far, here we showed the existence of the altered tunneling conductance at select boundaries on the surface by direct probing via the STM. The chemical nature of the enhanced activity at the grain boundaries is the subject of our ongoing investigation.

Integrating our results from the enhanced tunneling conductance on the grain boundaries with the thickness dependence of the grain growth due to heat treatment can provide valuable insights for the design of the infiltrated LSM cathodes (9). Based on these results, the infiltrated cathode film electrocatalytic activity and its durability could favor the presence of large number of the grain boundaries with a film thickness above few tens of nanometers.

Correlation of Surface Composition and Electron Tunneling: The temperature-dependent AES measurement in  $10^{-6}$  mbar oxygen pressure revealed enrichment of Sr and depletion of Mn and La on the surface, resulting in an overall 15-27% increase in the (La+Sr)/Mn ratio at 600-700°C (Fig.3). We attribute this evolution to a thermodynamically favored A-site cation-rich phase on the LSM surface during the AES experiment conditions. This observation is consistent with the results of prior experimental studies which report Sr segregation on the LSM surface (10,11) often accompanied by changes in the Mn valence state (12). Furthermore, these results are supported by recent *ab initio* hybrid density-functional calculations, (13) which predict the stable coexistence of (Sr,La)O- and MnO<sub>2</sub>-terminated surfaces at room temperature and the (Sr,La)O-terminated surfaces as energetically more favorable at 800°C on LSM.

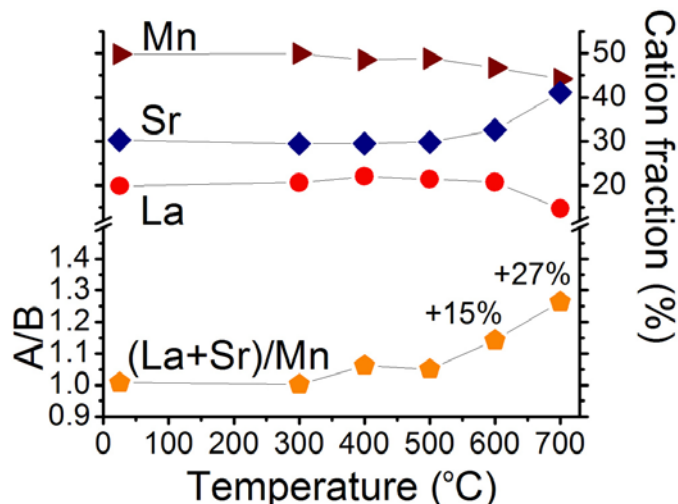


**Figure 3.** Temperature dependent AES revealed Sr enrichment, and Mn and La depletion at the surface above 500°C, with an increase in the (La+Sr)/Mn ratio.

The tunneling current measurements on LSM surface showed a semiconductor-like band-gap behavior at room temperature and a metallic nature at 400-580°C (Fig. 4), when the STS was collected with the acquisition time of 0.6ms per voltage step. An increase in the tunneling conductance was found as the temperature increased to 400°C and 500°C, followed by its decrease at 580°C. The initial increase in the tunneling conductance via the change from a large band-gap semiconducting to metallic behavior (Fig. 4) is not expected to be caused only by the thermal excitation of charge carriers at

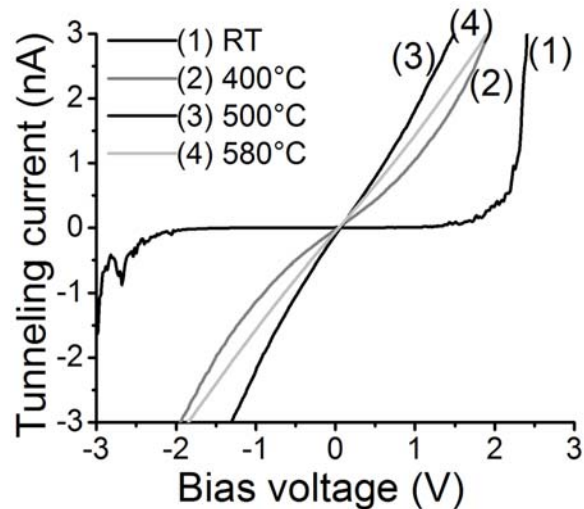


**Figure 4.** Tunneling current spectra on the surface of the 50nm LSM at room temperature, 400, 500 and 580°C with the acquisition time of 0.6ms per voltage step.

400°C, but could rather have an origin related to the role of surface oxygen defects upon heating. The nature of this transition remains unclear and a subject of our further investigation. On the other hand, the further increase in the tunneling conductance from 400 to 500°C could be attributed mainly to the effect of the elevated temperature on the electronic conductance of a semiconductor (14). The following decrease in the conductance at 580°C can result from the thermodynamically driven changes in the surface structure and composition of the LSM. Although no diffraction pattern was detectable with LEED in this work, we attributed this transition to a chemical change associated with Mn-depletion on LSM surface, as identified with AES results shown in Fig. 3.

Electronic conductance of the LSM is associated with the Mn cation and its oxidation state. A p-type conductivity in LSM arises as a result of hole-doping through the increase in  $\text{Mn}^{4+}/\text{Mn}^{3+}$  ratio, (15) which depends on the A-site cation substitution and oxygen non-stoichiometry. We attribute the decreasing tunneling conductance measured by STS at 580°C (Fig. 4) to the depletion of Mn on the surface at comparable conditions (Fig 3). This result suggests that the A-site rich and Mn-poor surfaces are less active for electron exchange in oxygen reduction on LSM. Although, the STS and AES experiments reported here were carried out at different oxygen pressures ( $10^{-3}$  mbar and  $10^{-6}$  mbar for STS and AES, respectively), both involved oxygen-poor environment at high temperature. Therefore, their comparison is expected to be qualitatively valid.

The Variation of STS Spectra: A broad distribution of the STS spectra was observed on the surface regardless of the grain boundaries at room temperature (Fig. 5). On the 50nm-thick LSM film, the band gap variation extended from 1.9 to 3.6eV, which goes far beyond the instrument related data dispersion (16). We tentatively attribute the broad range of band gap on LSM surface to two main mechanisms: 1) The abovementioned coexistence of the (Sr,La)O- and  $\text{MnO}_2$ -terminated surfaces: This is consistent with topographic and spectroscopic atomic-scale study of  $\text{Bi}_{0.24}\text{Ca}_{0.76}\text{MnO}_3$ , on which the phase separation into metallic and insulating surface regions were resolved in

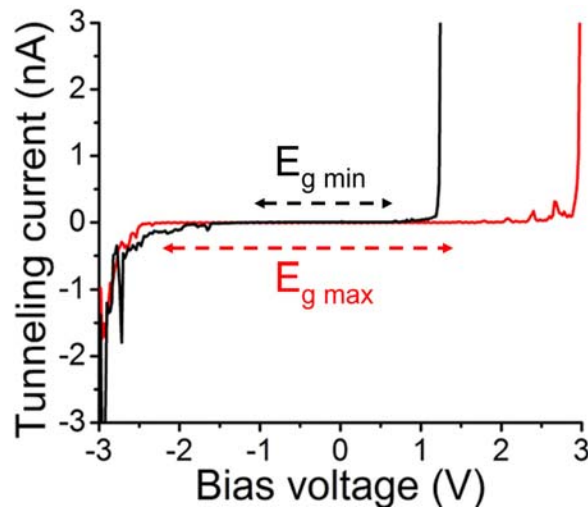


**Figure 5.** Tunneling current spectra, showing the broad range of the band gap energy that varies from 1.9eV to 3.6eV on the surface of the 50nm-thick LSM at room temperature.

real space with STM/STS at atomic-scale resolution (17). By taking the STM images and I-V spectroscopy simultaneously, the researchers showed that the charge order correlates with both structural order and the local conductive state, i.e. either metallic or insulating. These experiments provide an atomic-scale basis for descriptions of manganites as mixtures of electronically and structurally distinct phases. 2) Presence of electronic inhomogeneities on the surface due to defect ordering on perovskite-type oxides: This behavior was recently shown by imaging the  $\text{Mn}^{3+}$  and  $\text{Mn}^{+4}$  sites using STM at ambient temperature on  $(\text{La}_{5/8-0.3}\text{Pr}_{0.3})\text{Ca}_{3/8}\text{MnO}_3$  (18). The surface defects were reported to form strong short-range correlation with clear preference to exist as nanoscale charge-order-like clusters with varying electronic tunneling characteristics. While we propose that these two mechanisms could control the broad distribution of the I/V spectra on LSM reported here, the exact reasons are not yet fully identified.

Threshold Potential for LSM Surface Reaction with Oxygen: The STS measured within the  $-/+3\text{V}$  range with the 20ms acquisition time per voltage step at  $10^{-3}$ mbar oxygen pressure and elevated temperatures revealed a sudden drop in the tunneling current at a positive threshold bias (Fig. 6(a)). This differs from STS spectra acquired with the acquisition time of 0.6ms as shown in Figs. 4 and 5. The threshold bias decrease with increasing temperature is observed and estimated to 2.6, 2.3, and 1.5V at 400°C, 500°C, and 580°C, respectively (Fig. 6(b)). Similar threshold behavior was also observed on the 10 and 100nm-thick LSM films (not shown here). STM imaging and STS with the 0.6ms acquisition-time was fully recovered following the tunneling current drop, thus proving that the tip was not altered.

The acquisition-time-, temperature-, and bias-dependent character of the tunneling drop on LSM suggests that the underlying phenomenon is an activated chemical reaction. While here we report this behavior for the first time for a perovskite surface at high temperature, a similar tip-induced nanometric oxidation accompanied by the drop in tunneling conductance was extensively studied for Si and GaAs surfaces at room temperature (19,20). The observations were supported by an analytical model based on the Cabrera and Mott theory for the field-induced oxidation (21). On LSM surface, positive bias leads to an upward bending of the electronic bands (22) and shifts the cation

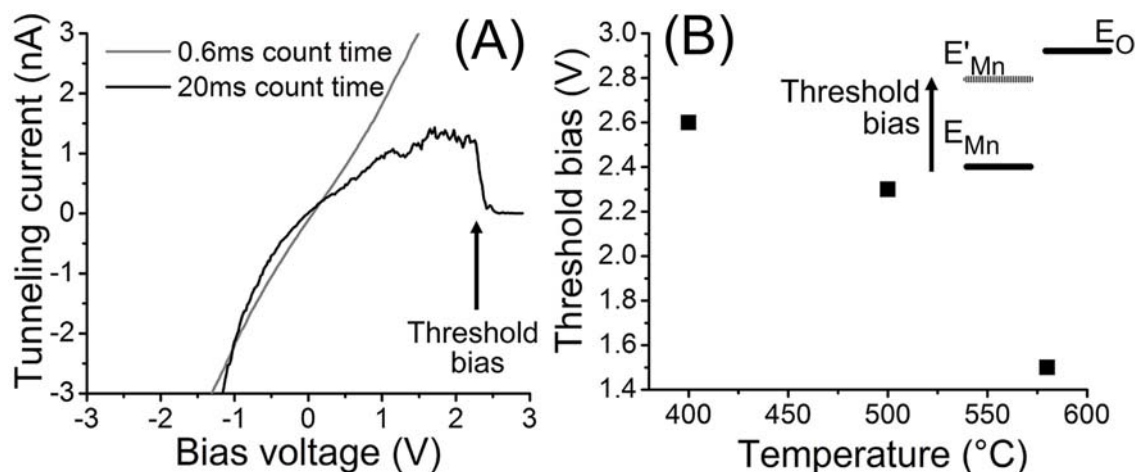


**Figure 6.** (a) Tunneling conductance spectra acquired on the surface of the 50nm-thick LSM at 580°C with 0.6 and 20ms acquisition time per voltage step, and (b) the threshold bias as a function of temperature. The inset in (b) schematically shows the cation energy levels ( $E_{Mn}$ ) shifting upward ( $E'_{Mn}$ ) at positive bias, and approaching the oxygen electronic levels ( $E_O$ ).

electronic states to higher energy levels, as schematically shown in inset of Fig. 6(b). The bias-induced band bending could be then responsible for the oxygen chemisorption localized at the tip – LSM surface at high temperature. The resulting formation of oxidized sites is a possible mechanism explaining the tunneling drop in STS. Recent *ab initio* studies (23) indicate that the favorable site for oxygen binding on LSM surface is atop Mn-cation. The valence band maximum of LSM (from -3 to 0 eV) consists of Mn(3d)-derived states that are split into  $t_{2g}$  and  $e_g$  bands, as identified with the photoemission spectroscopy (24, 25). Due to the p-type conductivity of LSM, the electron transfer to oxygen should take place from the  $t_{2g}$  levels (26). The upward band shift in the relative energies (Fig. 6(b)-inset) of these Mn(3d)-derived states can result in an increased catalytic activity for the reaction with oxygen from the gas phase (27). Based on this mechanism, we suggest that the threshold bias can serve as a unique probe of the activation polarization in cation-oxygen bonding on LSM cathode surface.

### Summary

In summary, we investigated the surface topography and the electronic properties of the LSM dense thin-film cathode surfaces using scanning tunneling spectroscopy, at high temperatures up to 580°C in oxygen gas environment. To the best of our knowledge, this is the first STM/STS investigation of LSM surfaces at high temperature and non-UHV conditions close to the reacting environment of operational SOFC cathodes. The main results reported here are: 1) significantly higher electron exchange on select grain boundaries compared to the grains surface, suggesting higher rate of the catalytic activity on them, particularly important information for tailoring the properties of infiltrated LSM cathodes; 2) thickness dependence of the grain growth that was caused by the heat treatment; 3) threshold-like drop in the tunneling current that was found at positive bias in STS, serving as a unique indicator of the activation polarization in cation-oxygen bonding on LSM surface; 4) Sr-enrichment and Mn-depletion on the surface at high temperature that was accompanied by a reduction in tunneling conductance in STS, suggesting that the Mn-terminated surfaces are more active for electron exchange in

oxygen reduction compared to the (La,Sr)-terminated surfaces on LSM. These findings can contribute to the atomistic-scale understanding of the electrocatalytic properties of the LSM cathode surfaces, and be a key for the rational design of the desirable cathode materials and structures for SOFCs.

### Acknowledgements

We thank Department of Energy, Office of Fossil Energy for financial support under award number DE-NT0004117, and Hoydoo You and Clemens Heske for constructive discussions. This work was performed in part at the Center for Nanoscale Systems (CNS), a member of the National Nanotechnology Infrastructure Network (NNIN), which is supported by the National Science Foundation under NSF award no. ECS-0335765. CNS is part of the Faculty of Arts and Sciences at Harvard University.

### References

- <sup>1</sup> S. C. Singhal, *Sol. St. Ionics*, **135** 305 (2000).
- <sup>2</sup> S. B. Adler, *Chem. Rev.*, **104** (10) 4791 (2004)
- <sup>3</sup> F. S. Baumann, J. Fleig, M. Konuma, U. Starke, H.-U. Habermeier, and J. Maier, *J. Electrochem. Soc.*, **152** (10) A2074 (2005)
- <sup>4</sup> V. Brichzin, J. Fleig, H.-U. Habermeier, G. Cristiani, and J. Maier, *Sol. St. Ionics*, **499** 152 (2002)
- <sup>5</sup> G. J. la O', B. Yildiz, S. McEuen, Y. Shao-Horn, *J. Electrochem. Soc.*, **154** (4) B427 (2007)
- <sup>6</sup> K. R. Balasubramaniam, S. Havlia, P. A. Salvador, H. Zheng, and J. Mitchell, *Appl. Phys. Lett.*, **91** 232901 (2007)
- <sup>7</sup> M. Petitjean, G. Caboche, E. Siebert, L. Dessemond, L.-C. Dufour *J. Eur. Ceram. Soc.*, **25** 2651 (2005)
- <sup>8</sup> R.A. De Souza, J.A. Kilner, J.F. Walker, *Mater. Lett.*, **43** 43 (2000)
- <sup>9</sup> T.Z. Sholklapper, V. Radmilovic, C.P. Jacobson, St. J. Visco, and L. C. De Jonghe, *Electrochem. and Sol. St. Lett.*, **10** (4) B74 (2007)
- <sup>10</sup> H. H. Kumigashira, K. Horiba, H. Ohguchi, K. Ono, M. Oshima, N. Nakagawa M. Lippmaa, M. Kawasaki, H. Koinuma, *Appl. Phys. Lett.*, **82** 3430 (2003).
- <sup>11</sup> R. Bertacco, J.P. Contour, A. Barthelemy, J. Olivier, *Surf. Sci.*, **511** 366 (2002).
- <sup>12</sup> M. Backhaus-Ricoult, *Sol. St. Ionics*, **177** 2195 (2006).
- <sup>13</sup> S. Piskunov, E. Heifets, T. Jacob, E. A. Kotomin, D. E. Ellis, and E. Spohr, *Phys. Rev. B*, **78** 121406R (2008)
- <sup>14</sup> K. Seeger, *Semiconductor physics: an introduction*, 9-th Edition Springer (2004)
- <sup>15</sup> C. Zener, *Phys. Rev.*, **82** 403 (1951)
- <sup>16</sup> N. Severin , S. Groeper, R. Kniprath, H. Glowatzki, N. Koch, I.M. Sokolov, J.P. Rabe, *Ultramicrosc.*, **109** 85 (2008)
- <sup>17</sup> Ch. Renner, G. Aeppli, B.-G. Kim, Yeong-Ah Soh S.-W. Cheong, *Nature*, **416** 518 (2002)
- <sup>18</sup> J. X. Ma, D. T. Gillaspie, E.W. Plummer, and J. Shen, *Phys. Rev. Lett.*, **95** 237210 (2005)
- <sup>19</sup> Y. Okada, Y. Iuchi, M. Kawabe, J. S. Harris Jr., *J. Appl. Phys.*, **88** 1136 (2000)
- <sup>20</sup> D. Stievenard , B. Legrand, *Progr. Surf. Sci.*, **81** 112 (2006)
- <sup>21</sup> J. A. Dagata, F. Perez-Murano, G. Abadal, K. Morimoto, T. Inoue, J. Itoh, and H. Yokoyama, *Appl. Phys. Lett.*, **76** 2710 ( 2000)

- 
- <sup>22</sup> R. M. Feenstra, Y. Dong, M. P. Semtsiv and W. T. Masselink, *Nanotech.*, **18** 044015 (7pp) (2007)
- <sup>23</sup> Y. Choi, M. C. Lin, and M. Liu, *Angew. Chem. Int. Ed.*, **46** 7214 (2007)
- <sup>24</sup> M. P. de Jong, V. A. Dediu, C. Taliani, W. R. Salaneck, *J. Appl. Phys.*, **94** 7292 (2003)
- <sup>25</sup> A. Chikamatsu, H. Wadati, H. Kumigashira, M. Oshima, A. Fujimori, N. Hamada, T. Ohnishi, M. Lippmaa, K. Ono, M. Kawasaki, and H. Koinuma, *Phys. Rev. B*, **73** 195105 (2006)
- <sup>26</sup> H. Kamata, Y. Yonemura, J. Mizusaki, H. Tagawa, K. Narayato and T. Sasamoto, *J. Phys. Chem. Solids.*, **56** 943 (1995)
- <sup>27</sup> Ph. Avouris, R. E. Walkup, A. R. Rossi, H. C. Akpati, P. Nordlander, T. -C. Shen, G. C. Abeln and J. W. Lyding, *Surf. Sci.* , **363** 368(1996)